Journal of Constructional Steel Research 126 (2016) 37–49

Contents lists available at ScienceDirect

Journal of Constructional Steel Research

Perforated metal shear panels as bracing devices of seismic-resistant structures

A. Formisano *, L. Lombardi, F.M. Mazzolani

Department of Structures for Engineering and Architecture, University of Naples "Federico II", P.le Tecchio 80, 80125 Naples, Italy

ARTICLE INFO

Article history:
Received 8 May 2015
Received in revised form 4 July 2016
Accepted 11 July 2016
Available online 15 July 2016

Keywords:
Steel Plate Shear Walls
Perforated panels
Circular holes
FEM model
Parametric analysis
Design charts

ABSTRACT

Steel Plate Shear Walls (SPSWs) are innovative systems able to confer to either new or existing structures a significant capacity to resist earthquake and wind loads. Many tests have shown that these devices may exhibit high strength, initial stiffness and ductility, as well as an excellent ability to dissipate energy. When full SPSWs are used as bracing devices of buildings, they may induce excessive stresses in the surrounding main structure where they are inserted, so to require the adoption of large cross-section profiles. For this reason, perforated steel panels, which are weakened by holes aiming at limiting the actions transmitted to the surrounding frame members, represent a valid alternative to full panels. In this work, aiming at showing the advantages of such devices, a FEM model of perforated panels has been calibrated on the basis of recent experimental tests. Subsequently, a parametric FEM analysis on different series of perforated panels, by changing the number and diameter of the holes, the plate thickness and the metal material, has been carried-out. Finally, the achieved numerical results have been used to set up an analytical tool to correctly estimate the strength and stiffness of perforated metal shear panels.

1. Introduction

The seismic protection systems based on the use of Steel Plate Shear Walls (SPSWs) consist of stiff horizontal and vertical boundary frame elements and infill plates. SPSWs possess good ductility and high energy dissipating capability under cyclic loading and they are also characterized by high initial stiffness, resulting very effectively in limiting the inter-storey drift of concrete or steel framed buildings. In addition, by using shop-welded or bolted connection type, the erection process can be facilitated, allowing a considerable reduction of constructional costs.

There are two types of SPSW systems, namely the "standard system" and the "dual system" [1]. In the "standard system", SPSWs are used as the lateral load resisting system, so beams and columns are designed to transfer vertical loads only. In the "dual system", also the boundary members, generating a moment resisting frame, contribute to resist lateral loads. Generally, these systems are located in perimeter frames of the main structure or around staircases, they occupying an entire span or a part thereof. Moreover, they can be stiffened or unstiffened, depending on the design philosophy. In the first case, SPSW may be provided with bending stiffeners, which improve the structure dissipative behaviour. Alternatively, the same behaviour can be attained by using low yield strength metals, namely low yield steel [2] or aluminium [3], as base materials for plates. When unstiffened thin panels are used, they immediately buckle under in-plane loads, but additional loads can be carried due to the tension-field mechanism, i.e. the development of tensile strips in the plate main diagonal direction [4]. From recent studies, it was found that the panel ideal behaviour is obtained for width/height ratios between 0.8 and 2.5 [5]. As a consequence, the boundary frame members have to be designed to support the tension-field mechanism developed by the plate. The tension-field action may induce in the frame members large forces demand, which gives rise to the adoption of high depth profiles. A number of solutions have been proposed to alleviate this condition, based on connection of the infill plate to the beams only [6], on vertical slits [7], on thin light-gauge cold-rolled steel [8], on low-yield strength steel [9,10], on perforated SPSW [11] and on aluminium plates [12,13].

In this paper, the attention is focused on the use of perforated SPSWs, in order to limit the construction costs deriving from their installation into the structure. Therefore, a FEM model, implemented with ABAQUS [14] and calibrated on the basis of previous literature experimental tests on panels with a central hole, has been developed in order to set up a parametric analysis on devices having different configurations of holes.

In conclusion, the achieved numerical results have been used to propose analytical tools under form of design charts for evaluating both the shear capacity and the initial stiffness of perforated metal shear panels.

2. Previous researches on unstiffened perforated panels

The first studies aimed at evaluating the behaviour of unstiffened steel panels were presented during the first '80s of the last century

* Corresponding author.
E-mail addresses: antoform@unina.it (A. Formisano), luca.lombardi.88@gmail.com (L. Lombardi), fmm@unina.it (F.M. Mazzolani).

http://dx.doi.org/10.1016/j.jcsr.2016.07.006
0143-974X/

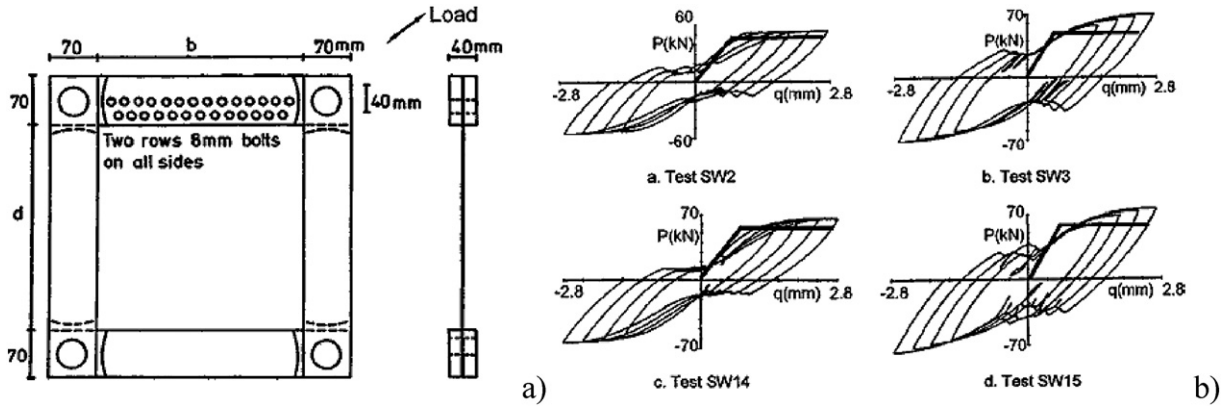

Fig. 1. Specimens tested by Roberts and Sabouri-Ghomi [16] (a) and their experimental cyclic responses with the equivalent bilinear diagrams provided by Eqs. (1) and (2) (b).

[15]. In 1991, on the basis of experimental diagonal tests performed on SPSWs within a pinned joint frame (Fig. 1), Roberts and Sabouri-Ghomi [16] proposed a theoretical method, namely the Plate-Frame Interaction (PFI) method, for calculating the shear capacity F_{wu} and the stiffness K_w of the steel plate device. The contribution of the plates only can be obtained through the following equations:

$$F_{wu} = b\,t\left(\tau_{cr} + \frac{1}{2}\,\sigma_{ty}\sin 2\vartheta\right) \tag{1}$$

$$K_w = \frac{\left(\tau_{cr} + \frac{1}{2}\,\sigma_{ty}\sin 2\vartheta\right)}{\left(\frac{\tau_{cr}}{G} + \frac{2\,\sigma_{ty}}{E\sin 2\vartheta}\right)}\frac{b\,t}{d} \tag{2}$$

where t, b, d are the thickness, width and height of the steel plate, respectively, E and G are the Young and shear elasticity moduli of the steel plate materials, σ_{ty} is the tension-field stress in the plate yielding condition, ϑ is the diagonal tension-field angle, measured from the

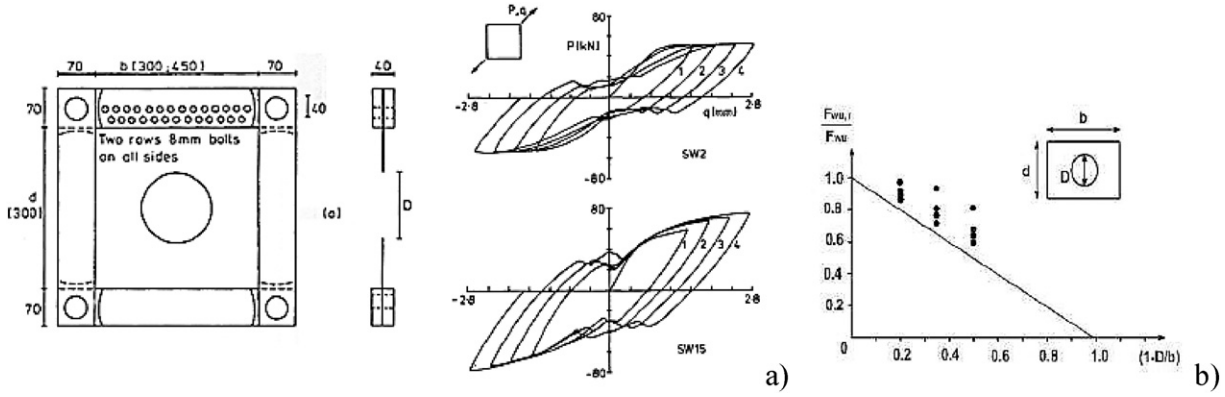

Fig. 2. Specimens tested by Roberts and Sabouri-Ghomi [18] (a) and linear reduction factor (b).

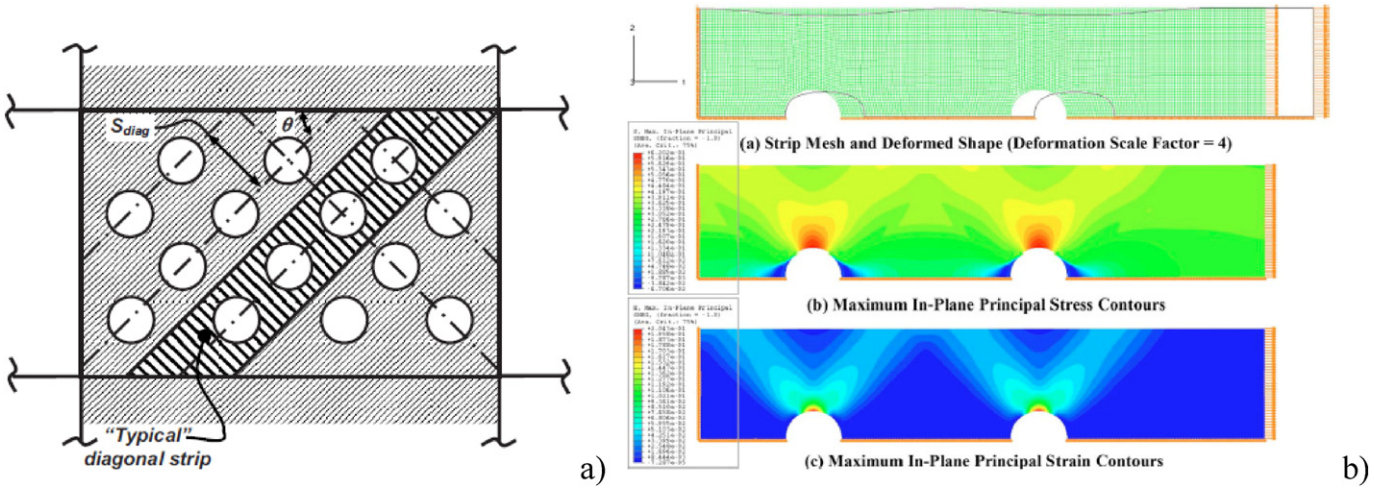

Fig. 3. The perforated SPSW studied by Purba and Bruneau [11] (a) and FEM analysis results on a perforated semi-strip (b).

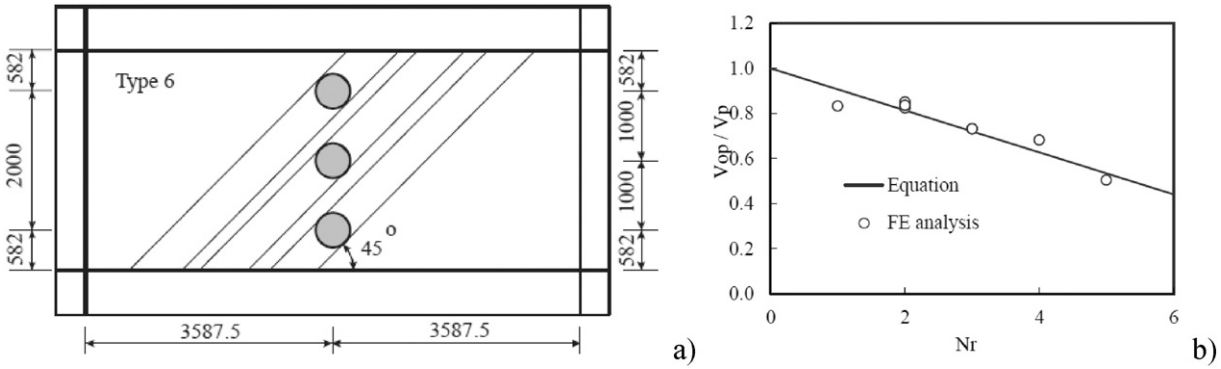

Fig. 4. Example of perforation layouts examined by Bhowmick et al. [20,21] (a) and comparison among theoretical and numerical results in terms of the plate shear strength (b).

vertical direction, and τ_{cr} is the critical buckling shear stress, evaluated according to the Timoshenko's theory [17].

Performing experimental tests on panels with a central opening (Fig. 2), Roberts and Sabouri-Ghomi [18] proposed an empirical reduction factor $(1-\frac{D}{d})$, where D is the opening diameter and d is the panel depth, for taking into account the decrease of SPSW strength and stiffness in Eqs. (1) and (2), respectively. The Authors also proposed to use a reduction coefficient $(1-\frac{A}{A_0})$, where A is the opening area and A_0 is the plate area, instead of the above one.

In 2005 Sabouri-Ghomi et al. [19] modified Eqs. (1) and (2) by introducing two modification factors, namely C_{m1} and C_{m2}, accounting for beam-to-column connections, plate-to-frame connections and the effect of both flexural behaviour and stiffness of boundary elements. By applying the above modification factors, Eqs. (1) and (2) became:

$$F_{wu} = b\,t\left(\tau_{cr} + \frac{C_{m1}}{2}\,\sigma_{ty}\sin 2\vartheta\right) \tag{3}$$

$$K_w = \frac{\left(\tau_{cr} + \frac{C_{m1}}{2}\,\sigma_{ty}\sin 2\vartheta\right)}{\left(\frac{\tau_{cr}}{G} + \frac{2\,C_{m2}\,\sigma_{ty}}{E\sin 2\vartheta}\right)}\frac{b\,t}{d} \tag{4}$$

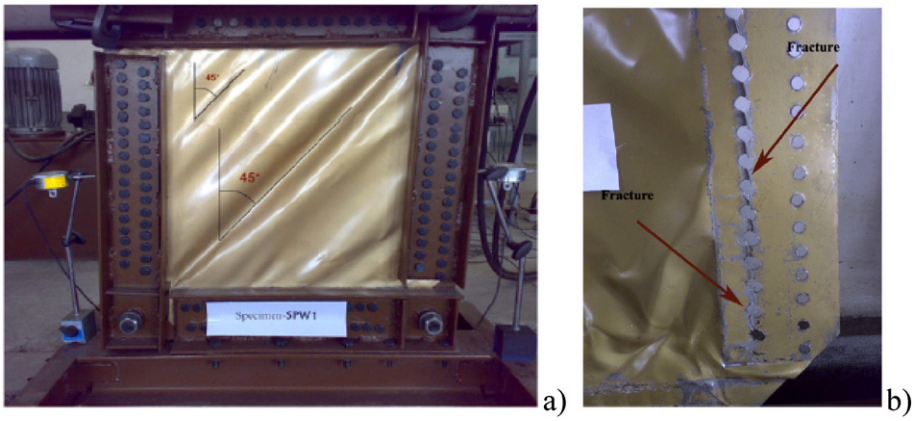

Fig. 5. Full panel deformed configuration (a) and failure mechanisms (b) at the end of the test conducted by Valizadeh et al. [22].

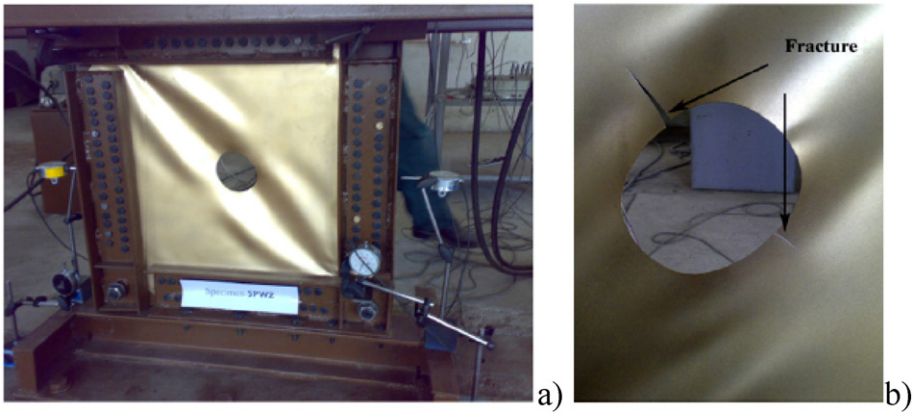

Fig. 6. Perforated panel deformed configuration (a) and tearing failure around opening (b) at the end of the test conducted by Valizadeh et al. [22].

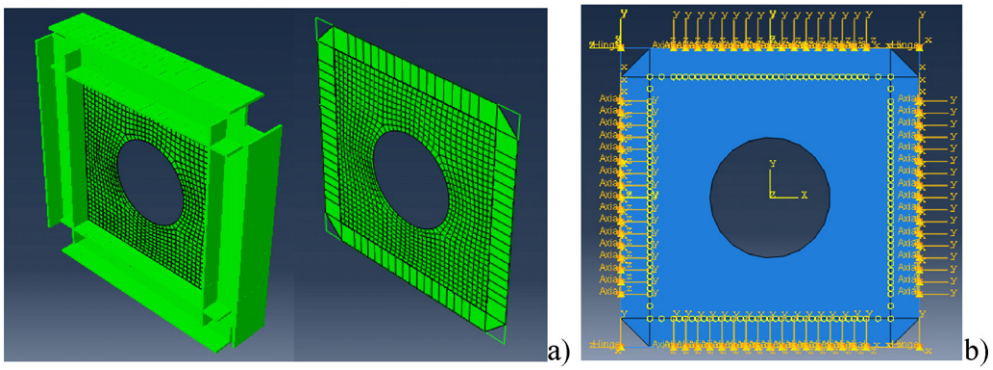

Fig. 7. Proposed FEM model: mesh (a) and boundary conditions (b).

where the modification factors were limited as follows: $0.8<C_{m1}<1.0$ and $1.0<C_{m2}<1.7$. The Authors recognised that these values will need further refinement as more test results will become available in the future.

Purba and Bruneau [11] experimentally tested a 4000 × 2000 mm shear panel with a configuration of 20 regularly spaced circular holes (Fig. 3). The panel, made of low yield strength steel, had reduced beam sections at the ends. Utilizing a thin panel with low yield strength, the Authors observed that both the device strength and energy dissipation was reduced as anticipated. It was also found that, for multiple regularly spaced perforations, Eq. (1) provided a conservative estimate of the perforated infill plate strength when d is replaced by S_{diag}, that is the diagonal distance between two consecutive perforation lines. So, through a FEM model calibrated on the experimental results, the following modified equation to calculate the shear strength of perforated shear panels with regular perforation patterns was proposed:

$$F_{wu,perf} = F_{wu}\left(1-0.7\frac{D}{S_{diag}}\right) \tag{5}$$

Moreover, by studying a plate portion, the researchers observed that analysis results on an individual perforated strip can accurately predict the behaviour of a complete perforated SPSW, provided that the hole diameter is less than 60% of the strip width.

A series of unstiffened SPSWs with different perforation patterns were investigated by Bhowmick et al. [20,21]. On the basis of analytical considerations, the Authors showed that the shear strength of an infill plate with circular perforations can be calculated by the following equation:

$$F_{wu,perf} = F_{wu}\left(1-\beta N_r\frac{D}{L_p\cos\alpha}\right) \tag{6}$$

where α is the tension-field angle, D is the circular hole diameter, L_p is the width of the perforated infill plate, N_r is the maximum number of diagonal strips and β is a regression constant, obtained from a FEM analysis, to fit the system behaviour. Eight perforation patterns and three diameters of the holes were considered. It was shown that a value of 0.7 can be assumed for the constant β, except for plates with a central hole, for which a value of 1.35 should be used. As a result, an excellent

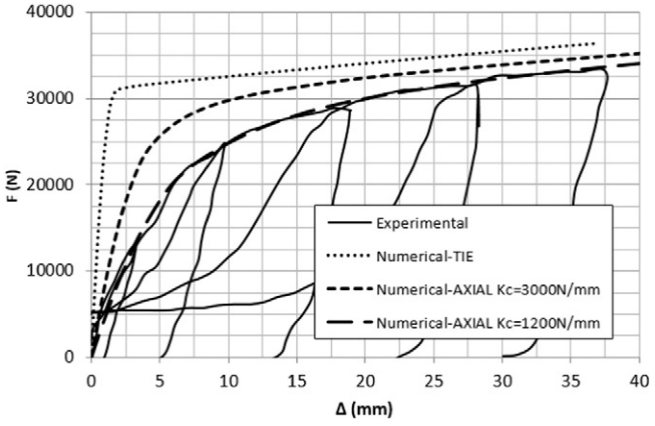

Fig. 8. Calibration of the connectors behaviour.

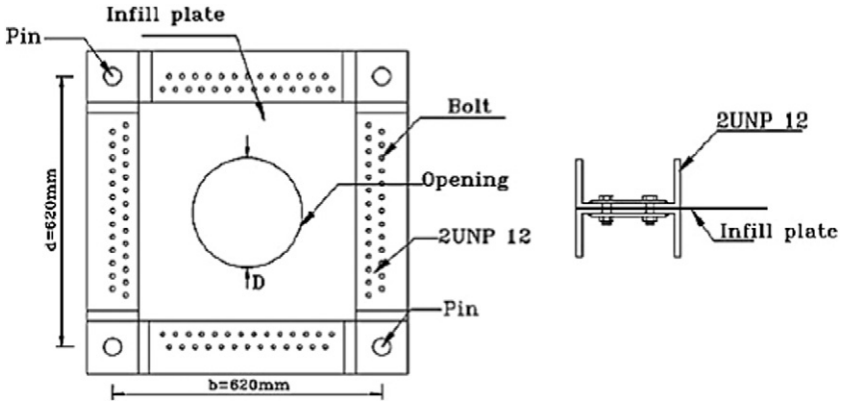

Fig. 9. Geometrical representation of the specimens tested by Valizadeh et al. [22].

Table 1
Features and failure modes of specimens experimentally tested by Valizadeh et al. [22].

Specimen	Thickness (mm)	Opening (mm)	f_{ym} (MPa)	f_{um} (MPa)	Failure mode
SPW1	0.70	/	180	300	Plate-frame connection
SPW2	0.70	100	180	300	No failure
SPW3	0.70	175	180	300	No failure
SPW4	0.70	250	180	300	No failure
SPW5	0.37	/	299	375	Plate-frame connection
SPW6	0.37	100	299	375	Fractures around hole
SPW7	0.37	175	299	375	Fractures around hole
SPW8	0.37	250	299	375	No failure

agreement between the FEM analysis results and the device shear strength prediction resulted from Eq. (6) was observed (Fig. 4).

In 2012, eight 1:6 scaled test specimens with a central circular hole, having two plate thicknesses and four D/b ratios (D = hole diameter and b = panel width), were tested under cyclic loading by Valizadeh et al. [22].

The obtained experimental results showed a stable behaviour of the panels for large displacements up to a drift of 6%. It was also observed that, during the loading phase, the stable cyclic behaviour of specimens in the non-linear range mostly causes a dissipation of energy, but the presence of an opening at the panel centre provoked a noticeable decrease in the system energy absorption. At the test program, specimens without opening, due to their higher ultimate strength, showed a bearing failure of the plate-to-connection system near the corner (Fig. 5). In perforated specimens with lower plate thickness, plate tearing failure occurred around the opening due to the stress concentration (Fig. 6).

3. Description of the proposed FEM model

The existing experimental studies on perforated SPSWs gave significant contributions to the understanding of the effective behaviour of such systems. However, the relevant geometrical and mechanical parameters of SPSW investigated in laboratory tests do not cover all possible panel configurations which can be used in practice. For this reason, a

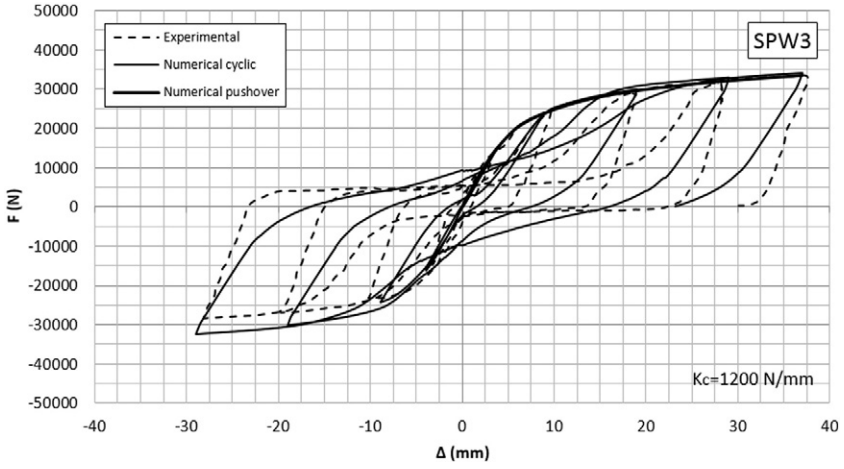

Fig. 10. Numerical calibration of experimental results on the SPW3 specimen tested by Valizadeh et al. [22].

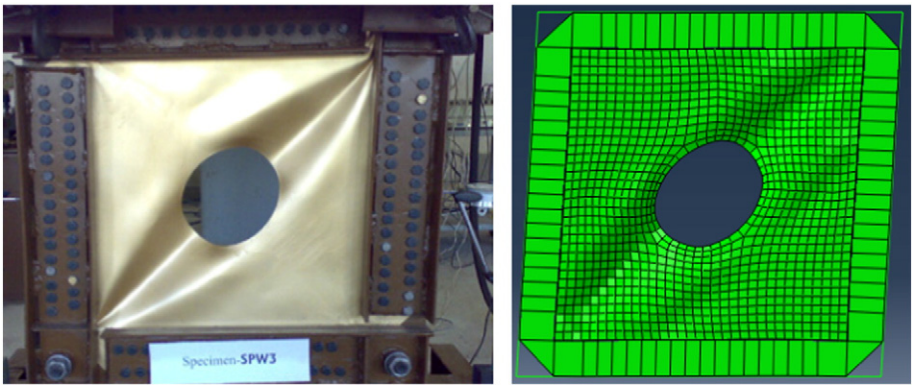

Fig. 11. Experimental-numerical comparison in terms of deformed shape for the SPW3 specimen tested by Valizadeh et al. [22].

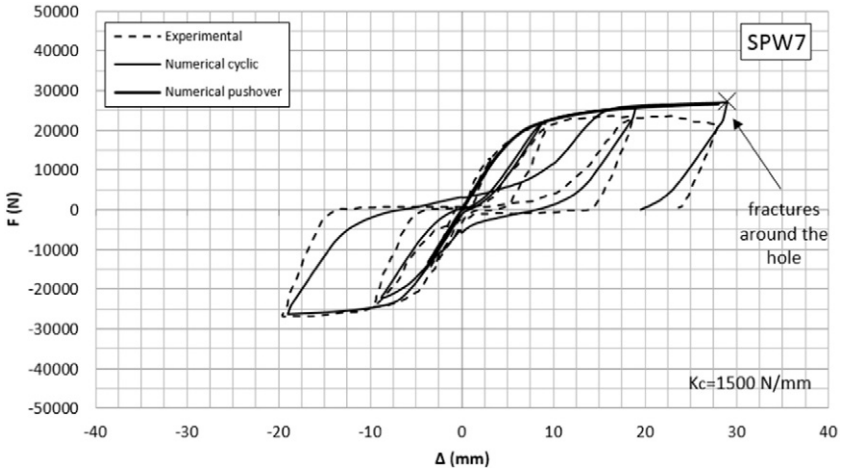

Fig. 12. Numerical calibration of experimental results on the SPW7 specimen tested by Valizadeh et al. [22].

FEM model is herein implemented in ABAQUS [14] for simulating the behaviour of shear panels under cyclic and monotonic loading. In order to focus attention on the behaviour of the plate only, the proposed FEM model has been setup on panels within pinned joint frames made of UPN120 coupled profiles as in the already mentioned experimental test of Valizadeh et al. [22].

Both the plate and the frame are modelled with 3D deformable elements. Plate is modelled by S4R shell elements, while frame is modelled with B31 beam elements (Fig. 7a). The beam-to-column frame connections are modelled by HINGE connectors. Through a preliminarily sensitivity analysis, an approximate mesh size of 15 mm has been chosen for the plate. Due to the presence of holes, a more dense mesh around them

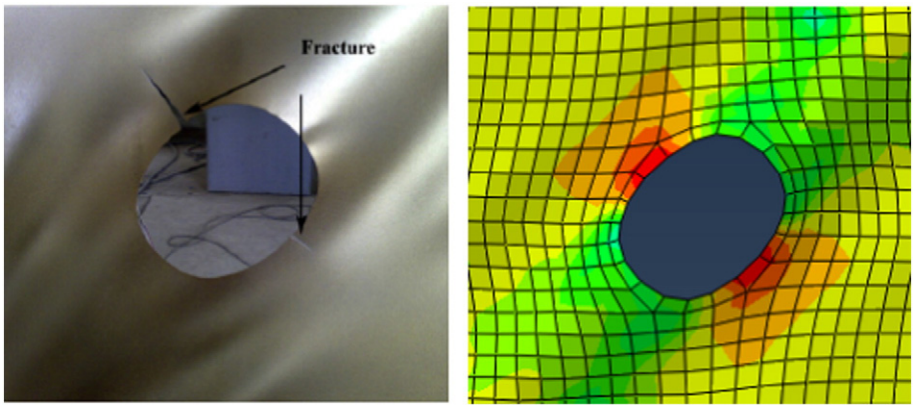

Fig. 13. Simulation of the stress concentration around the hole for SPW7 specimen tested by Valizadeh et al. [22].

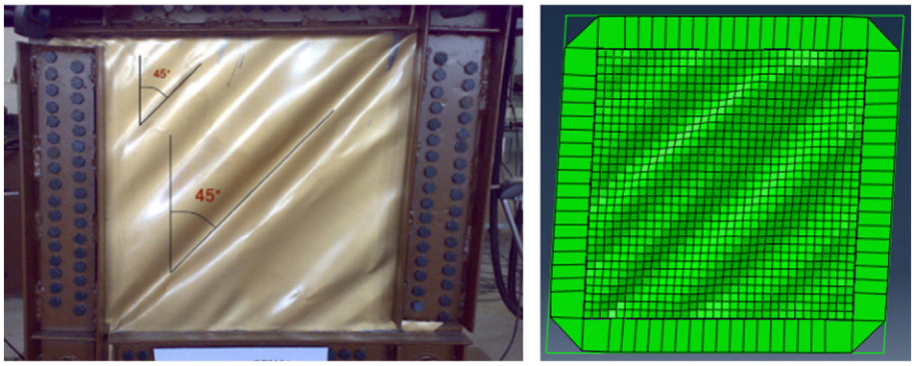

Fig. 14. Numerical calibration of the deformed shape of the SPW1 specimen tested by Valizadeh et al. [22].

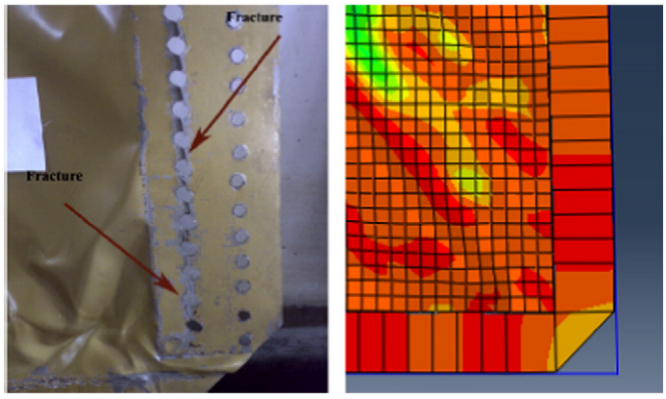

Fig. 15. Numerical simulation of the stress concentration in the SPW1 panel corners tested by Valizadeh et al. [22].

is required in order both to discretize properly the surface and to introduce a sufficient number of cells between near holes. About boundary conditions, at the base the frame is restrained with fixed hinges. Instead, the upper beam is constrained towards out-of-plane displacements in order to simulate the presence of lateral supports in that direction. The plate-to-frame connections are modelled by AXIAL connectors. For simplicity, an equivalent centroid row of connectors for each panel side, instead of the double rows used in the experimental test, is adopted (Fig. 7b). The contact between the two UPN120 profiles and the plate is simulated by restraining the out-of-plane displacement of the plate in an extended area of 60 mm from its edges. The mesh is diversified in this plate area, in comparison to that used for the plate, to reflect the real location of the bolts.

The model takes into account the geometrical and mechanical nonlinearity of the system. The plate is modelled by an elastic-plastic-hardening material. In particular, an isotropic hardening is used for the monotonic analysis, while a combined hardening is used for cyclic analysis on the basis of yielding stress and plastic strains of the plate material. The frame is modelled by an elastic material.

When plates are subjected to in-plane actions, their behaviour is affected by out-of-plane deformations. In fact, perfectly plane plates exhibit high stiffness under in-plane actions but, if affected by even small initial imperfections, they can exhibit substantially lower stiffness. These imperfections may be derived from either manufacture or installation processes. In order to take into account the initial imperfections, deformed shapes related to the plate instability modes are assigned to the SPSW. Moreover, some imperfections due to bolted connections localized along the panel perimeter (hole spacing, bolt-hole clearance, tightening pressure) have been introduced in the FEM model. It is possible to take into account for these imperfections by means of AXIAL connectors, whose behaviour is opportunely calibrated on the basis of the experimental evidences [22]. A sensitivity analysis has shown that, by using perfect plate-to-frame connections with the TIE function of ABAQUS, a stiffness greater than the experimental one is achieved. Contrary, first by properly calibrating the behaviour of the AXIAL connectors and then by assuming an initial imperfection of the plates with a deformed shape related to the first instability mode with amplitude equal to 1 mm, the experimental behaviour of the system has been realistically simulated (Fig. 8).

4. The FEM model calibration

The FEM model previously described has been calibrated by comparing the predictive behaviour to the test results of Valizadeh et al. [22]. This operation is necessary to take into account all imperfections and uncertainties that inevitably afflict the experimental reality. In these tests, eight panels filling a hinged joint frame have been considered. The centreline-to-centreline spacing between the two coupled UPN120 beams and columns of the frame has been set equal to 620 mm (Fig. 9). However, the geometrical dimensions of internal

Table 2
Summary of the results obtained from the model calibration.

Specimen	K_c (KN/m)	$K_{w,\exp}$ (KN/m)	$K_{w,num}$ (KN/m)	$VarK_w$ (%)	$F_{wu,\exp}$ (KN)	$F_{wu,num}$ (KN)	$VarF_{wu}$ (%)	$E_{d,tot,\exp}$ (KN/m)	$E_{d,tot,num}$ (KN/m)	$VarE_{d,tot}$ (%)
SPW1	1500	4870	5260	8	–	–	–	–	–	–
SPW2	1200	4400	4524	3	34.80	36.58	5	1.77	1.59	−11
SPW3	1200	4225	4057	−4	33.10	34.04	3	2.59	2.68	4
SPW4	1000	3866	3535	−9	25.00	25.52	2	1.70	1.54	−10
SPW5	1500	5118	4960	−3	–	–	–	–	–	–
SPW6	1300	3900	3801	−3	25.90	29.25	13	0.90	0.81	−11
SPW7	1500	4158	3765	−10	24.60	27.09	10	1.10	1.09	−1
SPW8	1500	4077	3255	−25	20.10	19.08	−5	1.10	0.83	−32

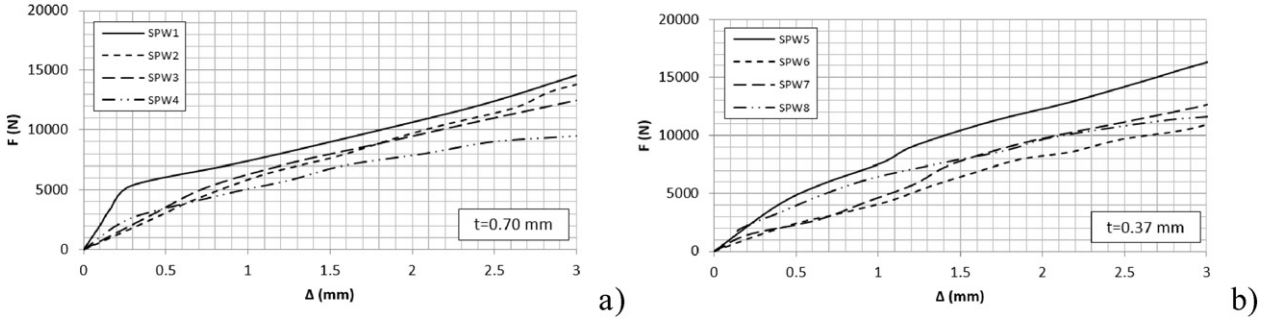

Fig. 16. Experimental initial curves of the panels tested by Valizadeh et al. [22].

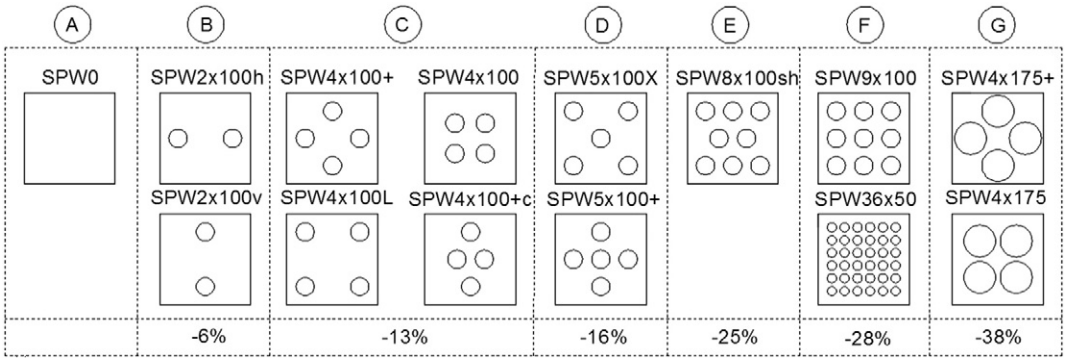

Fig. 17. Groups of analysed panels and identification of drilling percentages. The acronym SPW is followed by: the number of holes, the hole diameter (mm) and a symbol identifying the hole pattern (v: vertical, h: horizontal, L: large, +: vertical cross, c: close, X: diagonal cross, s: staggered).

plates have been assumed equal to 500 × 500 mm, by considering the depth of the applied channel sections of the framing system. The properties of experimental specimens are listed in Table 1. Experimental specimens have been tested under a cyclic loading process with five cycles up to a drift of 6%.

For the sake of brevity, just some of the obtained results are reported in the following. An initial out-of-plane imperfection proportional to the first instability mode with amplitude of 1 mm has been assigned to all panels. An elasto-plastic behaviour with combined hardening has been used for steel panels to perform numerical simulation in the cyclic field. The panel numerical behaviour has been experimentally calibrated on the basis of the axial stiffness of the connectors. In particular, the SPW3 panel has been calibrated by adopting a connector axial stiffness K_c equal to 1200 N/mm. This panel has shown, both experimentally and numerically, to attain a maximum drift of 6% without failure. The experimental-to-numerical comparison in terms of both hysteretic curves is shown in Fig. 10. The panel deformed shape is shown in Fig. 11.

The SPW7 specimen, more slender than the SPW3 one, has been calibrated by adopting a connector axial stiffness K_c of 1500 N/mm. This panel has shown, both experimentally and numerically, to attain a maximum drift of about 4% with fractures around the hole. From the experimental-to-numerical comparison in terms of F-Δ curve (Fig. 12), a little discrepancy is noticed in the post-peak strength phase. A better accuracy in the panel resistance prediction would be possible if the opening of fractures is modelled with a more refined theoretical model. However, the model is able to satisfactory simulate the stress concentration around the hole (Fig. 13).

The SPW1 panel has experimentally shown a failure at the plate-to-frame connections. This failure mode has strongly penalized its behaviour during the test. However, the initial behaviour of the panel before the failure has been simulated. This behaviour has been calibrated by adopting an extensional stiffness of the connectors K_c equal to 1500 N/mm. The tension-field development inside the plate before the failure

Table 3
Mechanical properties of materials used in the parametric analysis.

Material	E (MPa)	ν	f_y (MPa)	f_u (MPa)	ε_u
Steel	200,000	0.3	180	300	0.15
Aluminium (AW 1050 A)	70,000	0.3	18	70	0.35

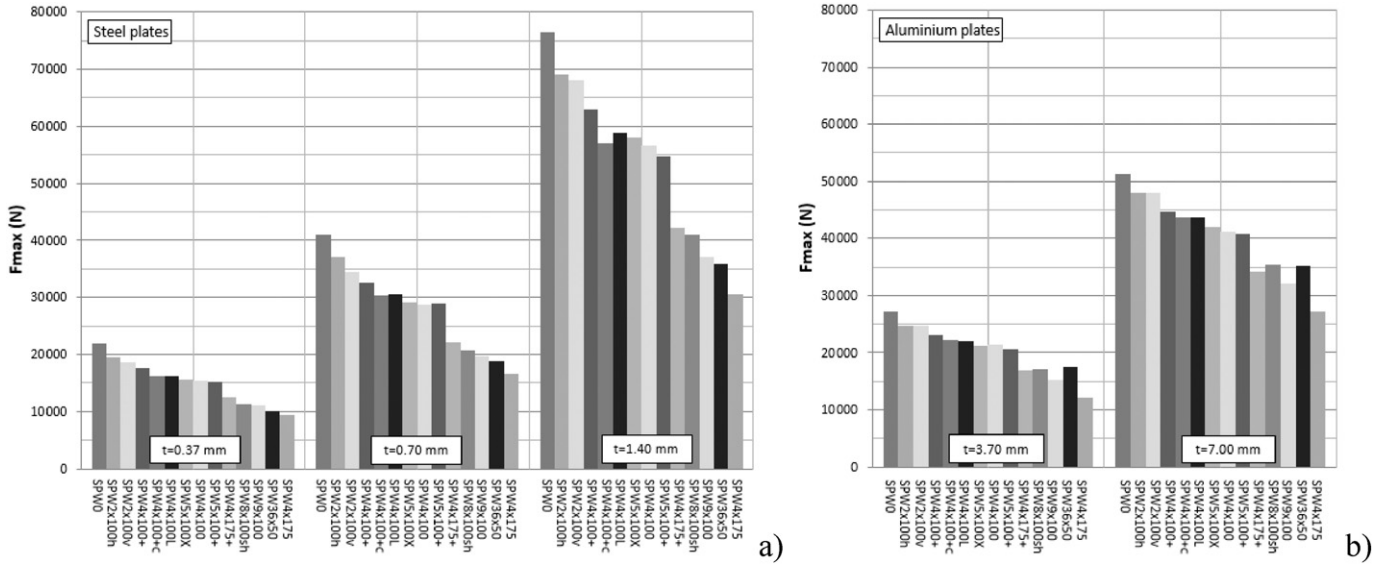

Fig. 18. Comparison between analysed steel (a) and aluminium (b) panels in terms of shear strength.

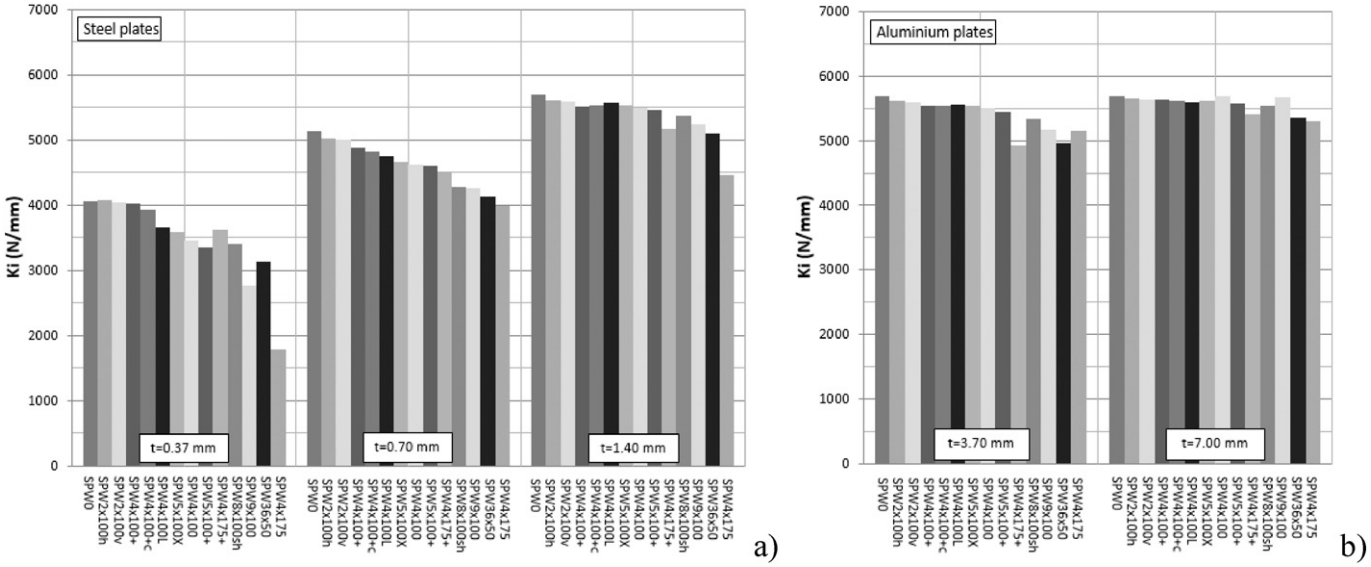

Fig. 19. Comparison between analysed steel (a) and aluminium (b) panels in terms of initial stiffness.

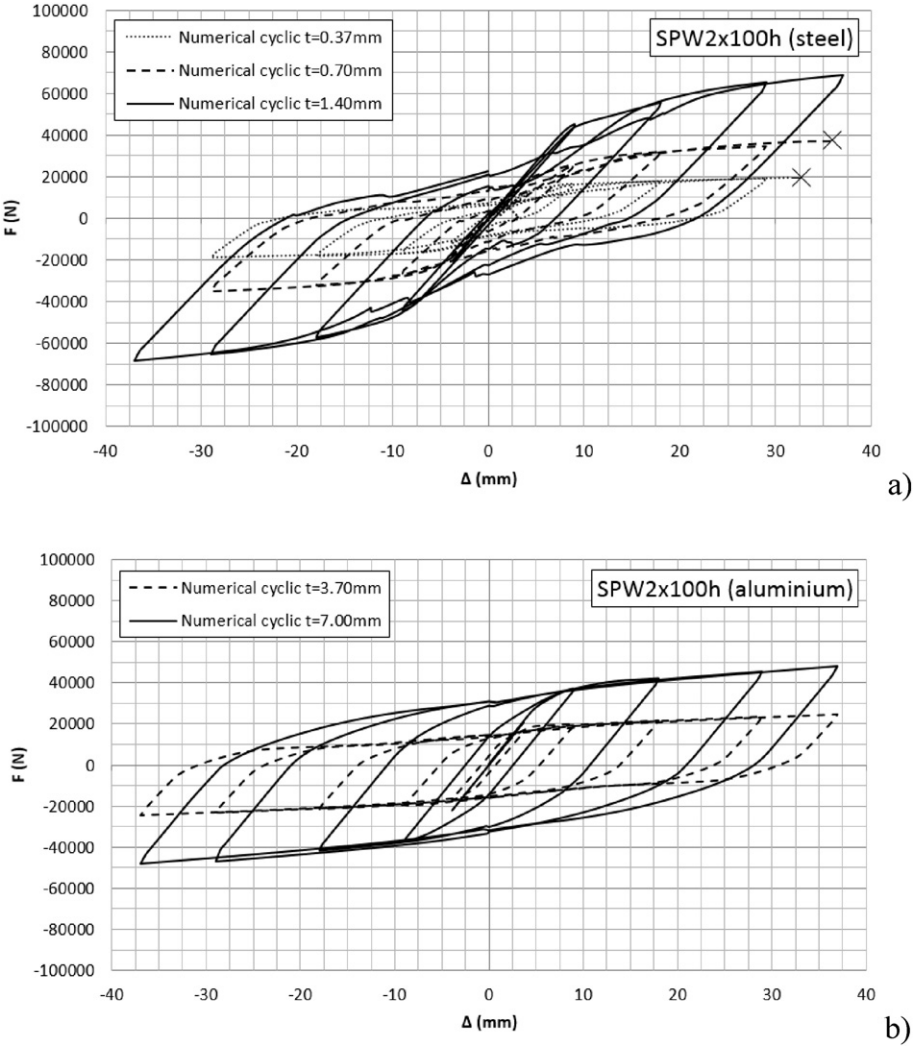

Fig. 20. Hysteretic curves of SW2x100h steel (a) and aluminium (b) panels with different thicknesses.

is shown in Fig. 14. Moreover, the FEM model is able to simulate the stress concentration in the panel corners (Fig. 15).

The final results of the calibration phase in terms of initial stiffness (K_w), shear strength (F_{wu}) and total energy dissipated during the testing process ($E_{d,tot}$) have been listed in Table 2. Since the experimental test results on the more slender panels have shown a dependence from both the initial buckling for low load levels and the initial slipping (i.e. SPW6 and SPW7 panels), a secant stiffness at a displacement of 3 mm has been conventionally assumed for a more realistic representation of the initial experimental behaviour of the panels. With these assumptions, the results have shown that the FEM model is able to satisfactory simulate the behaviour of shear panels in terms of stiffness, with the exception of SPW8 panel, which has experimentally shown a larger stiffness than that of the other panels with the same thickness, despite the presence of the greatest hole diameter (see Fig. 16b). The comparison between experimental and numerical results in terms of strength for SPW6 and SPW7 panels has shown a greater difference due to the lack of modelling of the fracture observed around the holes during the experimental tests (see Fig. 12). Less accuracy has been also observed in simulating the pinching effect, due to local instabilities occurrence. However, except for the SPW8 panel, the FEM model can be considered as sufficiently reliable, as it accurately estimates the three basic parameters (K_w, F_{wu}, $E_{d,tot}$) characterizing the physical behaviour of the panels coming from the experimental evidence.

5. Parametric analysis on perforated panels

A number of 13 different configurations of perforated shear panels have been analysed in the present study. These configurations differ from each other in terms of location, number and diameters of holes (Fig. 17), material (steel or aluminium) and plate thickness. In particular, following the dimensions of the specimens tested in [22], steel plates with a thickness of 0.37, 0.70 and 1.40 mm have been considered. In addition, aluminium plates with thickness of 3.70 and 7.00 mm have been also used in order to cover the same resistance range of steel panels.

The mechanical characteristics of the used materials are shown in Table 3.

Since the FEM model calibration has been done on the basis of some existing tests [22], the same steel quality has been adopted for parametric analyses. The mechanical properties of aluminium correspond to “ad hoc” material obtained by a thermal treatment, as suggested in [23], which lowers the elastic limit and amplifies the ultimate elongation. For cyclic tests the elasto-plastic behaviour with combined hardening has been used for steel and aluminium panel devices. The plate-to-frame connections are analogous to that used in [22], with a mean value of the connectors axial stiffness equal to 1200 N/mm. Any possible failure of the plate-to-frame connections has been considered. The plates initial imperfection has been given with an out-of-plane

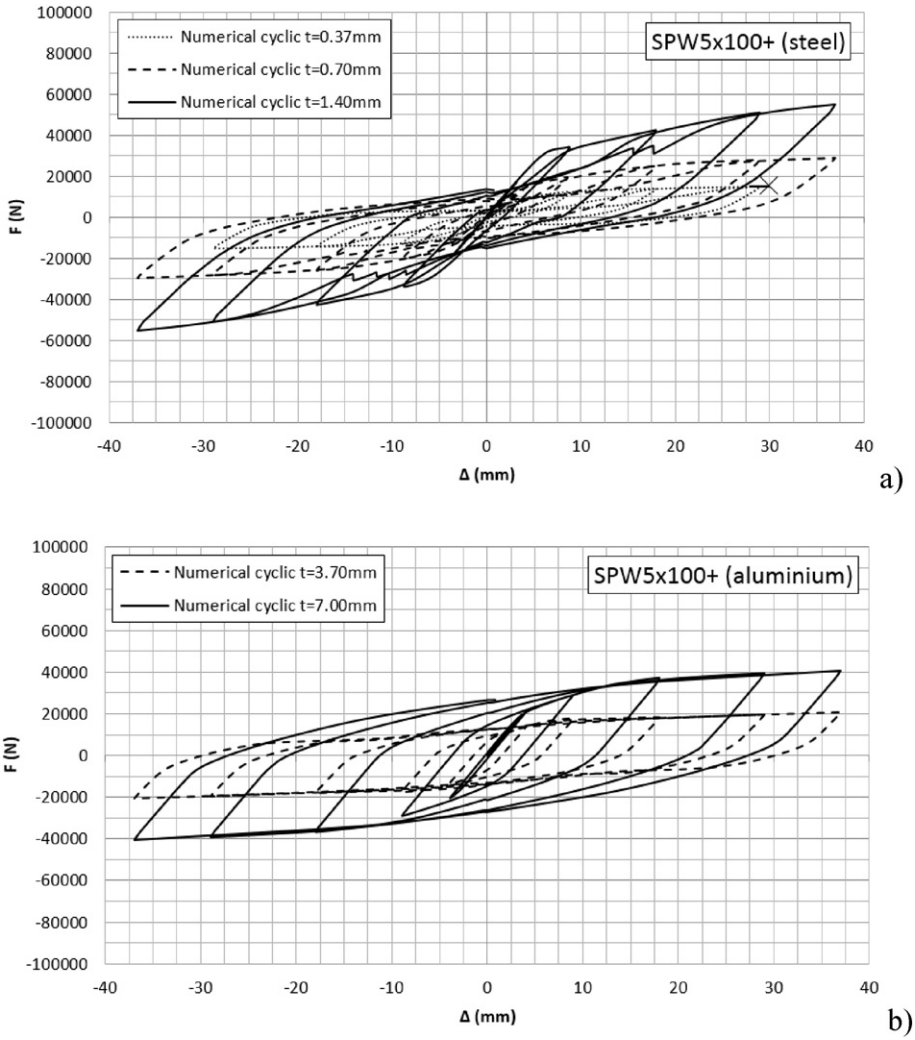

Fig. 21. Hysteretic curves of SW5x100+ steel (a) and aluminium (b) panels with different thicknesses.

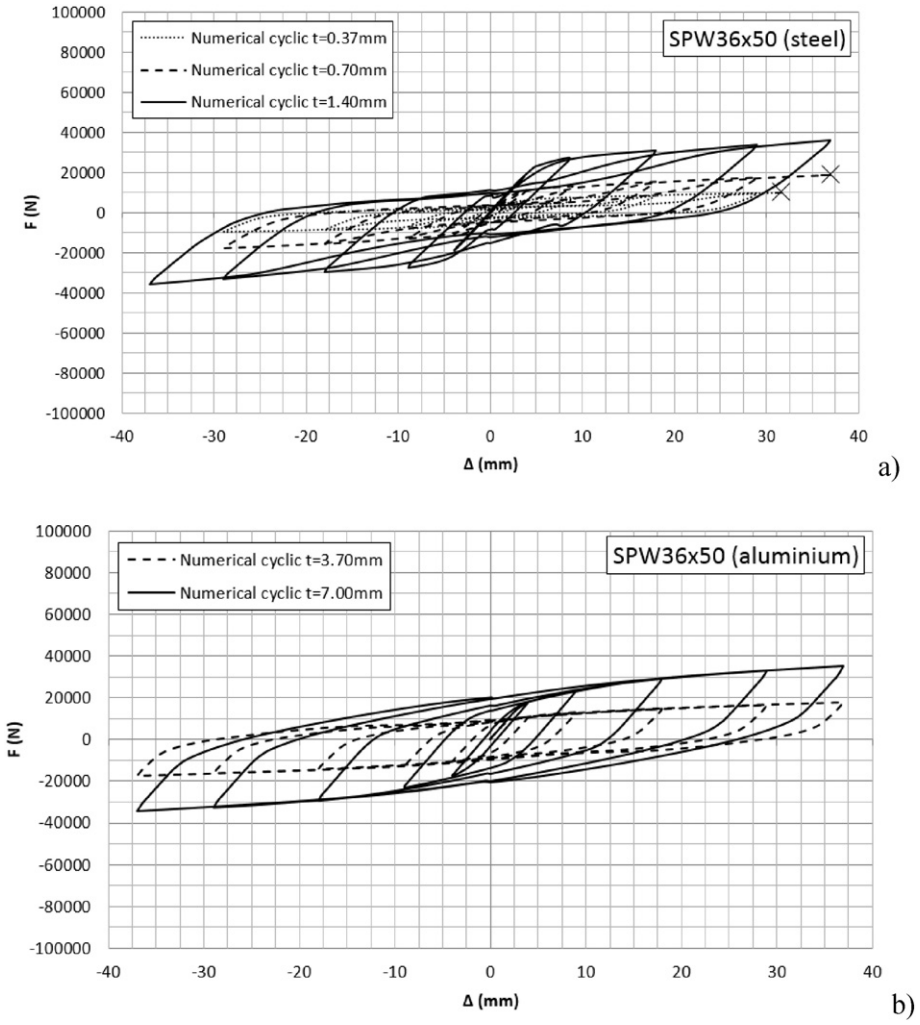

Fig. 22. Hysteretic curves of SW36x50 steel (a) and aluminium (b) panels with different thicknesses.

deformation having amplitude of 1 mm according to the panel first instability mode already considered in the previous FEM analysis phase. In the same way of the experimental tests, the FEM analyses have been pushed until either the creation of fractures around holes or the attainment of the maximum allowable displacement (drift of 6%).

Figs. 18 and 19 provide a summary of the contribution offered by perforated panels in terms of strength and initial stiffness, respectively. A large variety of shear strength contribution of perforated panels, lower than those offered by full panels, can be identified in these figures. This can be an advantage because the choice of a panel appropriate

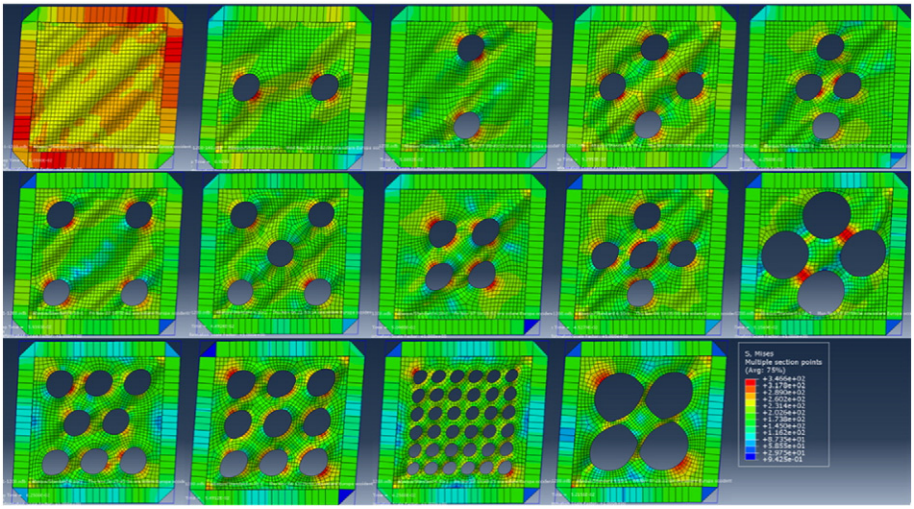

Fig. 23. Final stress and deformation states of the analysed steel shear panels with t = 0.70 mm.

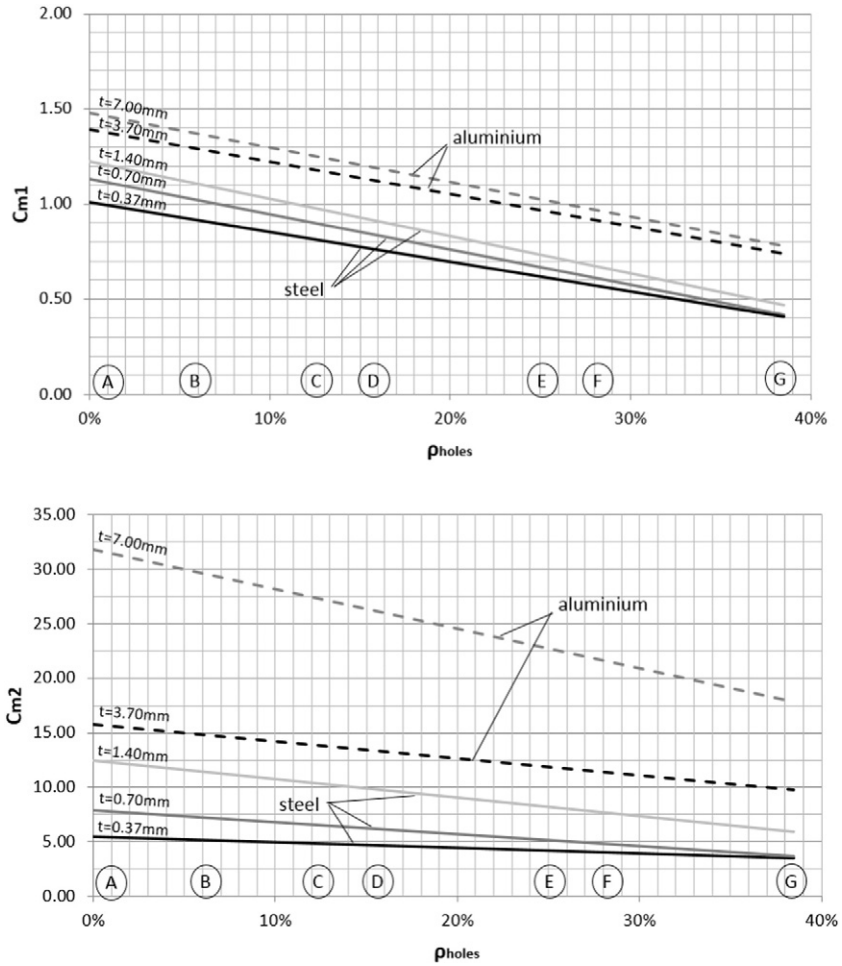

Fig. 24. Design charts for estimating the correction factors used to predict the non-linear behaviour of SPSWs.

drilling configuration can lead to the desired strength improvement requirement for the structure where panels are inserted.

The comparisons in terms of hysteretic curves for three panels having a percentage of holes ($\rho_{holes} = A_{holes}/A_{sup}$) equal to 6%, 16% and 28% are respectively reported in Figs. 20, 21 and 22. From these figures, it is noticed that aluminium panels have a better dissipative behaviour than the steel ones. For the former panels, the hysteretic cycles appear to be larger and characterized by a negligible pinching effect. In addition, thicker panels are susceptible to undergo high drifts without the formation of failures around holes. On the other hand, thinner steel plates have more tension field buckling upon load reversal, resulting in more pinched hysteresis cycles.

In Fig. 23 steel panels with t = 0.70 mm at collapse, due to either attainment of fracture around holes or fulfilment of ultimate displacement (37 mm) without failure, are shown. In this figure, despite the presence of holes that hinder the formation of the tension-field, the inclination of the tensile bands in all panels is substantially of 45°. Compared to full panels, the number of active bands decreases and it is reduced to one in the case of centred holes (i.e. SPW4x100 + c and SPW4x100). Furthermore, there is a different activation of the yielding mechanism with respect to full panels. In fact, yielding activates around the holes in perforated panels, without stressing the system joints, while yielding is activated in corner zones in full SPSWs, penalizing the connection systems. It is also possible to notice that, a considerable reduction of the stress state in the perimeter area is found in the perforated panels with a high percentage of hole.

The design charts reported in Fig. 24 are derived on the basis of the obtained numerical results. These charts can be used to evaluate the modification factor C_{m1} and C_{m2}, proposed by Sabouri-Ghomi [19] in Eqs. (3) and (4), to correctly predict the non-linear behaviour of perforated panels, in function of the thickness and the material. These factors have been obtained by assuming a simplified bi-linear force-displacement curve, which comes from the envelope of the numerical cyclic behaviour by compensating the areas (Fig. 25). In particular, for bilinearization method, the secant stiffness at a displacement of 3 mm, which is most representative of the post-buckling behaviour of the system, has been considered.

However, it is worth of noticing that these design charts are strictly valid for panels having the same geometry and material of those

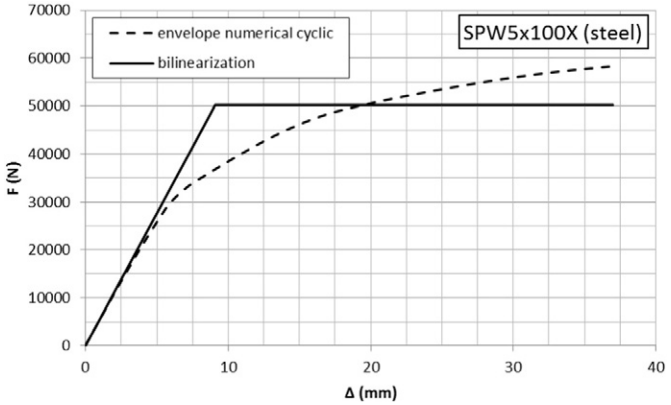

Fig. 25. Example of the numerical bilinear behaviour predicted for a SPSW.

considered in the parametric analysis. Therefore, additional studies should be developed to extend the achieved results to other cases.

Fig. 24 shows that the values of C_{m1} and C_{m2} assigned to aluminium panels are always higher than those used for steel ones. This trend can be explained as follows: the increasing of C_{m1}, which affects the strength (Eq. (3)), is due to the higher value of strain-hardening for aluminium; the increasing of C_{m2}, which affects the initial stiffness (Eq. (4)), depends on the lower value of the Young's modulus of aluminium respect to the steel one, being C_{m2} at the denominator in the formula.

6. Conclusions

The results of a wide FEM study on unstiffened perforated shear panels are presented in this paper. This paper represents a detailed extension of the contents already presented in [24]. The available experimental results on panels with a central opening have allowed to setup and calibrate an appropriate FEM model, where geometric imperfections and material non-linearity have been considered. The presence of the bolted plate-to-frame connections and their imperfections have been also simply taken into account in this model. The proper calibration of the FEM model has guaranteed to obtain a satisfactory numerical-to-experimental agreement in terms of both the overall behaviour and the consequential deformed shape of the system.

On this consolidated basis, a parametric FEM analysis on panels with different perforation patterns, material and thickness has been carried-out. The different perforation patterns have been considered by modifying location, number and diameter of the holes. Two types of material have been assumed: steel and aluminium. From the results it is observed that, despite the presence of holes, the inclination of tension-field essentially remains about 45°. The number of active bands decreases in comparison to the one full panels and it depends on the holes location, as also declared in [11]. Furthermore, the activation mode of the yielding mechanism is favourable for perforated panels, as it occurs in the areas around the holes instead of the perimeter zones like in full panels, which penalize the connection systems. A considerable reduction of the stresses in the perimeter area is found in perforated panels with a high percentage of holes. In addition, by adopting thicker perforated plates, very large drifts can be attained without failure around holes. In conclusion, the aluminium panels showed a more dissipative behaviour than steel panel ones, with the hysteretic curves afflicted by a negligible pinching effect.

Finally, it is shown that the use of conventional steel panels with different perforation patterns can be a viable alternative to full panels for strengthening and stiffening both new and existing structures. In fact, if perforated panels are applied for example to an existing structure, by choosing an appropriate drilling configuration, the resistance of the original building can be improved without overloading the main structure with high stresses deriving from the tension-field generated in the plates. Furthermore, due to weakening effect induced by the holes in the plates, perforated panels, other being more economic than full ones, require, when applied into existing buildings, less local reinforcement interventions to structural members in comparison to those imposed by full panels.

References

[1] A. Astaneh-Asl, Seismic behaviour and design of steel shear walls, Steel Technical Information and Product Services Report, Structural Steel Educational Council, Moraga, CA, 2000.
[2] G. De Matteis, A. Formisano, F.M. Mazzolani, S. Panico, Design of low-yield metal shear panels for energy dissipation, Proc. of the Final Conference of COST ACTION C12, Innsbruck, Austria January 20–22 2005, pp. 665–675.
[3] A. Formisano, F.M. Mazzolani, G. Brando, G. De Matteis, Numerical evaluation of the hysteretic performance of pure aluminium shear panels, Proc. of the 5th Int. Conference on the Behaviour of Steel Structures in Seismic Areas (STESSA '06), Yokohama, Japan, Taylor & Francis Group plc, London, UK August 14–17 2006, pp. 211–217.
[4] K. Basler, Strength of plate girders in shear, J. Struct. Div. ASCE 87 (7) (1961) 150–180.
[5] A. Formisano, F.M. Mazzolani, G. De Matteis, Numerical analysis of slender steel shear panels for assessing design formulas, Int. J. Struct. Stab. Dyn. 7 (2007) 273–294.
[6] M. Xue, L.W. Lu, Interaction of infilled steel shear wall panels with surrounding frame members, Proc. Annual Task Group Technical Session, Structural Stability Research Council: Reports on Current Research Activities, Lehigh University, Bethlehem, PA June 20, 1994, pp. 339–354.
[7] T. Hitaka, C. Matsui, Experimental study on steel shear wall with slits, J. Struct. Eng. 129 (5) (2003) 586–595.
[8] J.W. Berman, M. Bruneau, Experimental investigation of light-gauge steel plate shear walls, J. Struct. Eng. 131 (2) (2005) 259–267.
[9] D. Vian, M. Bruneau, Steel plate shear walls for seismic design and retrofit of building structures, Technical Rep. No. MCEER-05-0010, Multidisciplinary Center for Earthquake Engineering Research, State Univ. of New York, Buffalo, N.Y., 2005
[10] E.S. Mistakidis, G. De Matteis, A. Formisano, Low yield metal shear panels as an alternative for the seismic upgrading of concrete structures, Adv. Eng. Softw. 38 (2007) 626–636.
[11] R. Purba, M. Bruneau, Design recommendations for perforated steel plate shear walls, Technical Rep. No. MCEER-07-0011, Multidisciplinary Center for Earthquake Engineering Research, State Univ. of New York, Buffalo, N.Y., 2007
[12] A. Formisano, G. De Matteis, F.M. Mazzolani, Numerical and experimental behaviour of a full-scale RC structure upgraded with steel and aluminium shear panels, Comput. Struct. 88 (2010) 1348–1360.
[13] G. De Matteis, A. Formisano, F.M. Mazzolani, An innovative methodology for seismic retrofitting of existing RC buildings by metal shear panels, Earthq. Eng. Struct. Dyn. 38 (2009) 61–78.
[14] Hibbitt, Karlsson, and Sorenson, ABAQUS/CAE User's Manual, Version 6.10, HKS Inc., Pawtucket, RI, 2010.
[15] L.J. Thorburn, G.L. Kulak, C.J. Montgomery, Analysis of steel plate shear walls, Struct. Eng. Rep. No. 107, Dept. of Civ. Eng., University of Alberta, Edmonton, Alta., Canada, 1983.
[16] T.M. Roberts, S. Sabouri-Ghomi, Hysteretic characteristics of unstiffened steel plate shear panels, Thin-Walled Struct. 14 (1991) 145–162.
[17] S.P. Timoshenko, J.M. Gere, Theory of Elastic Stability, McGraw-Hill Book Company, 1961.
[18] T.M. Roberts, S. Sabouri-Ghomi, Hysteretic characteristics of unstiffened perforated steel plate shear panels, Thin-Walled Struct. 14 (1992) 139–151.
[19] S. Sabouri-Ghomi, C.E. Ventura, M.H.K. Kharrazi, Shear analysis and design of ductile steel plate walls, J. Struct. Eng. 131 (2005) 878–889.
[20] A.K. Bhowmick, Seismic behaviour of steel plate shear walls with centrally placed circular perforations, Thin-Walled Struct. 75 (2014) 30–42.
[21] A.K. Bhowmick, G.Y. Grondin, R.G. Driver, Nonlinear seismic analysis of perforated steel plate shear walls, J. Constr. Steel Res. 94 (2014) 103–113.
[22] H. Valizadeh, M. Sheidaii, H. Showkati, Experimental investigation on cyclic behaviour of perforated steel plate shear walls, J. Constr. Steel Res. 70 (2012) 308–316.
[23] G. De Matteis, A. Formisano, F.M. Mazzolani, S. Panico, Numerical and experimental analysis of pure aluminium shear panels with welded stiffeners, Comput. Struct. 30 (2008) 545–555.
[24] A. Formisano, L. Lombardi, F.M. Mazzolani, On the use of perforated metal shear panels for seismic-resistant application, 8th International Conference on Behavior of Steel Structures in Seismic Areas, Shanghai, China, July 1–3 2015.